Design of Membrane-Inserting Peptides: Spectroscopic Characterization with and without Lipid Bilayers†

L. A. Chung* and T. E. Thompson

Department of Biochemistry, University of Virginia School of Medicine, Charlottesville, Virginia 22908

Received January 16, 1996; Revised Manuscript Received June 28, 1996⊗

ABSTRACT: This paper reports the spectroscopic characterization of two *de novo* peptides. The first sequence, Ala peptide = H_2N-Ala_{27}-Tyr-Lys_6-$CONH_2$, gives circular dichroism (CD) and Fourier transform infrared (FTIR) spectra characteristic of β structure in solution, binds to lipid bilayer vesicles poorly, and tends to precipitate in buffered 0.1 M salt solutions. In the second sequence, Leu peptide = H_2N-Ala_2-Leu_3-Ala_{22}-Tyr-Lys_6-$CONH_2$, three leucines are substituted for three alanine residues. This small sequence change results in CD spectra that are characteristic of helical structures, while the FTIR spectra give evidence for complex equilibria between multiple structures in solution. The Leu peptide does not precipitate in buffered salt solutions and binds to lipid bilayers. The polarized attenuated total reflectance infrared spectra provide evidence of a transmembrane orientation for the helical peptide in lipid bilayers. The collective spectroscopic results are summarized in a tentative model in which the Leu peptide exhibits multiple equilibria between extended unordered, helix, and coiled-coil structures in solution; when lipid vesicles are added, the peptide binds to the lipid surface and then inserts into the lipid in a transmembrane orientation. The slow kinetics exhibited by the peptide suggest multiple conformational changes during the lipid−peptide interactions. The design rationale for the peptides is included in an appendix.

The question of how hydrophobic protein sequences partition into lipid bilayer membranes is a complex problem relevant to the biogenesis of membrane proteins. Certain proteins (e.g., apocytochrome *c*, cytochrome b_5) do not require special conditions such as a proteinaceous secretion machinery, transmembrane potential, or low pH for their insertion into lipid bilayers. This little-understood class of proteins uses a posttranslational, spontaneous-insertion mechanism to incorporate into membranes (Shore *et al*., 1995). A similar example is the *sec*-independent pathway in *Escherichia coli* whereby some integral inner membrane proteins do not require a fully functional translocation complex or protonmotive force for integration into the inner membrane (von Heijne, 1994).

Protein partitioning from a polar into nonpolar environment can be found in mammalian systems, where membrane proteins must move from the hydrophilic core of a translocon, which is a proteinaceous pore complex in the endoplasmic reticulum membrane, into the hydrophobic lipid membrane during biogenesis. A. E. Johnson and co-workers, in an examination of the molecular steps involved in protein movement through the translocon (Crowley *et al*., 1994), have recently obtained evidence suggesting that when the sequence becomes hydrophobic, the nascent chain is released from the pore into the surrounding lipid environment (S. Liao, J. Lin, and A. E. Johnson, personal communication).

We are studying the problem of spontaneous protein insertion into membranes using model systems composed of synthetic peptides and lipid bilayers of defined composition. The use of designed rather than biological peptide sequences has certain advantages [for an excellent short review see Sander (1991)]. The main advantage is an ability to test in a stringent manner predictions of structural requirements and the relationships between amino acid sequence, structure, and function. The analysis can be simplified by including residues appropriate for labeling by optical probes or by excluding residues that can interfere with biophysical and biochemical characterization of the system. The capacity to modify easily designs for medical or industrial applications is an added advantage. We report here two designed peptide sequences, Ala peptide = H_2N-Ala_{27}-Tyr-Lys_6-$CONH_2$ and Leu peptide = H_2N-Ala_2-Leu_3-Ala_{22}-Tyr-Lys_6-$CONH_2$. Only the Leu peptide is both soluble in aqueous solution and capable of interacting with uncharged lipid bilayers composed of phosphatidylcholines at the peptide concentrations studied. The peptides have been characterized using circular dichroism (CD),[1] Fourier transform infrared (FTIR), and attenuated total reflectance infrared (ATR-IR) spectroscopy to deduce the solution structures, membrane-bound secondary structures, and their orientation in a lipid bilayer. This paper reports the analysis of our spectroscopic results, discusses the requirements and rationale for the peptide design, and proposes a tentative model for the binding and insertion of these peptides into lipid bilayers. Portions of this work have been reported previously (Chung & Thompson, 1995, 1996).

† This work was funded by NIH Grant GM-14628.

* Corresponding author.

⊗ Abstract published in *Advance ACS Abstracts,* August 15, 1996.

[1] Abbreviations: Leu peptide, peptide with sequence $Ala_2Leu_3Ala_{22}$-TyrLys$_6$; Ala peptide, peptide with sequence Ala_{27}TyrLys$_6$; MALDI-TOF MS, matrix-assisted laser desorption ionization time-of-flight mass spectrometry; FTIR, Fourier transform infrared spectroscopy; ATR-IR, attenuated total reflectance infrared spectroscopy; CD, circular dichroism spectroscopy; POPC, 1-palmitoyl-2-oleoylphosphatidylcholine; DPPC, 1,2-dipalmitoylphosphatidylcholine; LUV, large unilamellar vesicles; Tris-HCl, tris(hydroxymethyl)aminomethane buffer adjusted with HCl; HEPES, *N*-(2-hydroxyethyl)piperazine-*N*′-2-ethanesulfonic acid; pD, pH meter reading for buffers in D_2O, these measurements were not corrected for activity of the deuterium ion; TFA, trifluoroacetic acid.

S0006-2960(96)00080-3 CCC: $12.00

MATERIALS AND METHODS

Materials. The lipids used in all experiments were obtained from Avanti Polar Lipids Inc. (Birmingham, AL) and stored at either −20 or −80 °C until use. Reagents used for peptide synthesis were obtained from Milligen/Biosearch (Burlington, MA), Bachem Fine Chemicals (Torrance, CA), and Calbiochem/Novobiochem (La Jolla, CA) and stored at −20 °C. Solvents used for purification were HPLC-grade; solvents used during the synthesis were either HPLC-grade, when available, or reagent-grade. All solvents were purchased from Aldrich Chemical Co. (Milwaukee, WI) or EM Science (Cherry Hill, NJ). All other chemicals (buffers, assay reagents, etc.) were purchased from both Aldrich Chemical Co. and Sigma Chemical Co. (St. Louis, MO).

Buffer Compositions and pH. The various buffers used for experiments were 100 mM HEPES in D_2O (FTIR buffer), pD = 7.7, which was used for the temperature-dependent infrared spectroscopy only, and 100 mM Tris-HCl or 50 mM Tris-HCl in D_2O, pD = 7.7, which were used for both circular dichroism and infrared spectroscopies at ambient temperatures. The HEPES buffer was used for temperature studies because of its greater temperature stability relative to Tris buffers. A third buffer system containing 5 mM hydrogen phosphate buffer with 100 mM NaF in D_2O (high-salt buffer), pD = 7.7, or 5 mM hydrogen phosphate buffer only in D_2O (low-salt buffer), pD = 7.7, were used for preliminary circular dichroism studies and are mentioned in the section on peptide solubility (see RESULTS). The pH of buffers in D_2O (pD) were measured at room temperature and not corrected for deuterium ion activity.

Peptide Synthesis and Purification. The peptides were synthesized using standard procedures for solid-phase FMOC chemistry. Automated synthesis was carried out using a Biosearch peptide synthesizer, Model 9600, for residues 1−29. The sequences were then completed manually on small aliquiots of peptide/resin that had been removed from the automated synthesizer, washed, lyophilized, and stored at −20 °C until needed. Coupling reactions were monitored by ninhydrin assays and residues were recoupled when necessary. In agreement with a previous report, we found that a lower substituted resin (0.15 vs >0.19 mequiv/g of resin) resulted in fewer truncation and/or deletion sequences as judged by the number of HPLC peaks and the MALDI-TOF MS (matrix-assisted laser desorption ionization time-of-flight mass spectrometry) results obtained for crude peptides after cleavage (Iwamoto *et al*., 1994).

The reverse-phase HPLC purification of the peptides was done using a Vydac C-18 column with a TFA/acetonitrile/water solvent system. Purified peptides were identified using MALDI-TOF MS. For infrared spectroscopy, the peptides were dialyzed exhaustively against 10 mM ammonium bicarbonate, pH = 7.8, to remove TFA and lyophilized before use (Surewicz & Mantsch, 1989).

FTIR Spectroscopy. Infrared spectra were measured using a Nicolet 740 instrument with an MCTA detector. For temperature-dependent FTIR spectra, samples were incubated in and spectra recorded from a thermostated cell described previously (Doebler & Holloway, 1993). The spacers used in the cell, and therefore the cell path length, varied from 25 to 50 μm. Infrared spectra were normally the average of 2000 scans. In a typical experiment, the sample was prepared by adding 100 mM HEPES buffer or buffer with lipid vesicles to the dry peptide in a small eppendorf tube. The sample was then mixed and allowed to stand at either room temperature or 15 °C for at least 24 h to ensure solution of the peptide. The sample was then introduced into the thermostated IR cell and incubated at the starting temperature of 15 °C for at least 2 h before the first set of scans was started. The temperatures were jumped in the order 15-25-37-45-37-25-15 °C (increasing−decreasing temperature scans) with appropriate incubation times at each temperature before collecting spectra. For some samples, increasing−decreasing−increasing and decreasing−increasing−decreasing cycles of various periods were also used to determine the incubation times required to bring the samples to equilibrium. It was found that incubation times as short as 2 h were adequate for peptides in aqueous buffer or peptides that did not interact with lipid. Peptide samples in the buffer with lipid vesicles were ratioed against background samples containing only buffer and vesicles; samples without lipid were ratioed against buffer-only background samples.

For the FTIR spectra at ambient temperatures, the samples prepared for circular dichroism were used (see below) and therefore the buffer system was Tris-HCl in D_2O (see above for details). An unthermostated, variable path length FTIR cell was used with either a 25- or 50-μm spacer. Other details of the experimental protocol were the same as for the temperature-dependent studies described above.

Polarized ATR-IR Spectroscopy. The equipment used for the preparation of single bilayers mounted on gemanium plates and the recording of ATR-IR spectra have been described in detail elsewhere (Frey & Tamm, 1991; Fringeli, 1993; Goormaghtigh & Ruysschaert, 1990). All procedures were carried out at ambient temperature (approximately 21−25 °C). Briefly, the germanium plate coated with a monolayer of lipid was placed in the ATR cell and the cell was sealed. A buffer solution containing palmitoyloleoylphosphatidylcholine large unilamellar vesicles (POPC LUV) was injected into the cell and allowed to incubate with the monolayer for 4 h. The cell was then washed with buffer to remove any unfused vesicles and background spectra were recorded for parallel- and perpendicular-polarized light. After the lipid-only spectra were recorded, peptide dissolved in buffer was injected into the cell and the peptide solution was allowed to incubate for 24 h with the lipid bilayer. The cell was then washed with fresh buffer to remove peptide which was not bound to the lipid bilayer, and the peptide plus lipid spectra were recorded. Four thousand spectra were collected and averaged for each polarization.

Circular Dichroism Spectroscopy. The circular dichroism spectra were collected using a Jasco 720 spectropolarimeter and a 0.01-cm path length cell. Cells with a longer path length resulted in greater noise at the required concentration of buffers. A bandwidth of 1.0 nm and step resolution of 0.2 nm were used to collect the average of 32 scans/sample at ambient temperature. The peptide spectra shown have the background buffer scans subtracted but were not smoothed or otherwise processed with noise reduction routines. The effect of the single tyrosine residue was estimated by collecting CD spectra for concentrations of tyrosine in buffer comparable to the peptide concentrations. Corrections due to the absorbance of this residue were minimal at the path length used (0.01 cm), had no effect on the final peptide spectra, and were therefore not subtracted.

Curve-Fitting of Infrared Spectra. The infrared spectra ratioed against background scans were fit using Spectra Calc (Galactic Industries Corp., Salem, NH). Only the amide I region of the spectra, 1700−1600 cm^{-1}, was used in the curve-fitting procedures; absorbance in the amide II region of 1600−1500 cm^{-1} was minimal in the D_2O-based buffers used (Holloway & Buchheit, 1990). H_2O vapor peaks were subtracted from ratioed spectra interactively when necessary. Spectra were smoothed using a Savitsky−Golay smoothing procedure with a factor of 13 and regions outside the 1700−1600-cm^{-1} range were deleted. Increasing the spectral window to 1760−1500 cm^{-1} to ensure a flat baseline resulted in the same peak positions and peak heights. After smoothing, spectra were corrected for sloping baselines and offset to place the minimum absorbance value at zero. Initial estimates of peak positions were made from the fourth derivatives of the spectra. No constraints were placed on the curve-fitting routine. Fitting was carried out until minimum χ^2 values were obtained; final χ^2 values are reported in the figure legends.

RESULTS

Solubility of the Peptides. Peptide solubility was determined using the turbidity of the solution or precipitation of the peptide as a rough measure. All peptide solutions up to 10 mg/mL (approximately 0.3 mM peptide), with one exception, were initially turbid to the eye but cleared within a few hours at room temperature. We ascribe this slow rate of solvation to the hydrophobicity of the sequences. Only the Ala Peptide in a high-salt buffer (see Materials and Methods) precipitated out of solution, although it was soluble in all other buffers. This peptide−high-salt buffer solution was initially turbid at 5 mg/mL Ala peptide, cleared slightly after about a half hour, and then slowly precipitated out over the course of a few hours at room temperature. After centrifugation, some peptide did remain in solution, but at a final concentration of less than 0.5 mg/mL, judging from the CD absorbance and the inability to obtain IR spectra with this sample. In contrast, the Leu peptide both dissolved well in high-salt buffer at all concentrations and gave a CD spectrum similar to the spectra shown in Figure 4. We also note that 1 mg/mL Ala peptide also precipitated out of the high-salt buffer in the presence of 100 mM lipid vesicles.

Circular Dichroism of Ala Peptide in Aqueous Solution. Initially when dissolved the Ala peptide shows helical CD spectra (data not shown). Over a period of hours the CD changes to give the spectra shown in Figure 1 for the Ala peptide at three different concentrations: 10 mg/mL = 3.5 mM (top panel), 2 mg/mL = 0.7 mM (middle panel), and 0.2 mg/mL = 0.07 mM (bottom panel). While the spectrum for the highest concentration of Ala peptide (top panel) was truncated at 200 nm due to detector saturation by the signal amplitude, the general features of the spectrum are clearly similar to those recorded for the lower concentrations of peptide. All three spectra have a single ellipticity minimum at 216−218 nm and the lower concentrations of peptide (two lower panels) have maxima at 196 nm while the highest concentration seems to approach a similar maximum. The circular dichroism spectra are indicative of β secondary structures (Perczel *et al*., 1992; Ono *et al*., 1990; Osterman & Kaiser, 1985). It should also be noted that the shapes of the spectra do not change with increasing peptide concentration, indicating no concentration dependence for the solution structure of the Ala peptide.

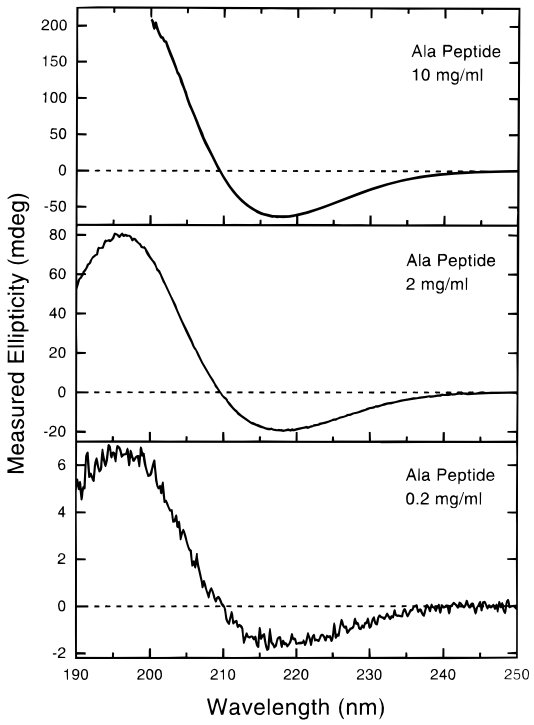

FIGURE 1: Concentration-dependent circular dichroism spectra for the Ala peptide at ambient temperature in D_2O buffer containing 100 mM Tris-HCl, pD = 7.7. Top panel: 10 mg of peptide/mL = 3.5 mM Ala peptide. Middle panel: 2 mg of peptide/mL = 0.7 mM Ala peptide. Bottom panel: 0.2 mg of peptide/mL = 0.07 mM Ala peptide. Sample preparation and CD measurements are described under Materials and Methods.

FTIR Spectroscopy and Curve-Fitting Analysis of Ala Peptide in Aqueous Solution. To correlate the circular dichroism results with the infrared spectroscopy, we collected FTIR spectra using the same samples. Figure 2 shows the concentration dependence of the FTIR spectra for the Ala peptide at ambient temperature. Only the two highest concentrations of Ala peptide, 10 mg/mL (3.5 mM, top panel) and 2 mg/mL (0.7 mM, bottom panel), gave reasonable spectra; the spectrum for the lowest concentration was very noisy and considered unreliable, especially after subtraction for water vapor (not shown). As seen for the CD spectra, the FTIR spectra of the two concentrations are the same shape, although the absorbencies differ as expected for the different concentrations.

The temperature dependence for the structure of the Ala peptide in solution was also characterized using FTIR spectroscopy. Figure 3 shows the FTIR spectra collected at 15, 25, 37, and 45 °C for 10 mg/mL Ala peptide in a HEPES/D_2O buffer, pD = 7.7 (top panel; see Materials and Methods for details). As shown in Figure 3, top panel, the spectra collected at the different temperatures overlay each other. It is concluded that the solution structures of the Ala peptide are independent of temperature over the range studied.

The bottom panel of Figure 3 shows the curve-fit analysis for the spectrum collected at 45 °C. The match of the original spectrum (dashed line) with the sum of the fitted curves (dotted line) and the low final χ^2 value of 2.1×10^{-5} indicate a reasonable fit for the spectrum using five peaks. The peak parameters and their assigned structures are listed in Table 1 while the structural assignments are discussed in

Table 1: Results of Curve-Fitting Analysis for FTIR and ATR-IR Spectra

sample (method)	temp (°C)	peak position (cm^{-1})	structural assignments[a]	peak height	peak area	% of total peak area
Ala peptide in buffer, 10 mg/mL (FTIR)	45	1623	β structure	0.047	0.449	17.26
		1627	β structure	0.048	1.233	47.35
		1650	unassigned	0.021	0.537	20.63
		1673	ap β	0.012	0.297	11.42
		1687	ap β	0.009	0.087	3.33
Leu peptide in buffer, 10 mg/mL (FTIR)	15	1622	β structure	0.040	0.368	7.73
		1627	β + ex + CC	0.067	1.702	35.73
		1651	helix	0.065	2.268	47.61
		1676	β + ex	0.017	0.353	7.40
		1689	ap β	0.007	0.072	1.52
Leu peptide in buffer, 10 mg/mL (FTIR)	45	1622	β structure	0.038	0.360	7.45
		1627	β + ex + CC	0.060	1.578	32.68
		1653	helix	0.076	2.575	53.34
		1677	β + ex	0.013	0.231	4.78
		1688	ap β	0.008	0.084	1.75
Leu peptide in buffer, 1 mg/mL (FTIR)	15	1635	ex + CC	0.008	0.216	46.97
		1653	helix	0.007	0.137	29.88
		1669	extended	0.004	0.106	23.16
Leu peptide in buffer, 1 mg/mL (FTIR)	45	1636	ex + CC	0.007	0.185	38.47
		1655	helix	0.009	0.204	42.31
		1671	extended	0.004	0.092	19.22
Leu peptide + 300 mM POPC (FTIR)	45	1621	β structure	0.020	0.315	7.88
		1649	unordered	0.076	3.149	78.69
		1653	helix	0.032	0.538	13.44
Leu peptide + POPC, perpendicular polarization (ATR-IR)	RT	1629	β structure	0.004	0.039	1.24
		1645	unordered	0.067	2.726	87.53
		1656	helix	0.019	0.350	11.22
Leu peptide + POPC, parallel polarization (ATR-IR)	RT	1629	β structure	0.004	0.043	0.74
		1645	unordered	0.100	4.070	70.32
		1658	helix	0.077	1.675	28.94

[a] RT = room temperature; ap β = antiparallel β-sheet; extended = extended unordered; β + ex = β-structure + extended unordered; β + ex + CC = β-structure + extended unordered + coiled coil; ex + CC = extended unordered + coiled coil.

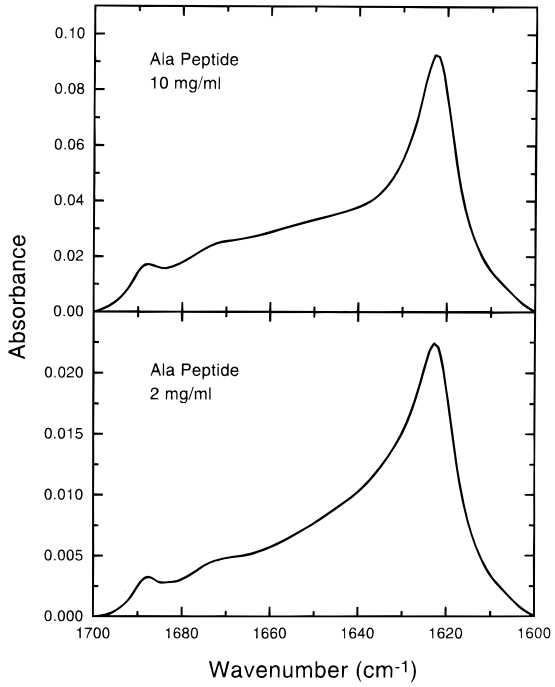

FIGURE 2: Concentration-dependent FTIR spectra for the Ala peptide at ambient temperature in D_2O buffer containing 100 mM Tris-HCl, pD = 7.7. Top panel: 10 mg of peptide/mL = 3.5 mM Ala peptide. Bottom panel: 2 mg of peptide/mL = 0.7 mM Ala peptide. Sample preparation and FTIR measurements are described under Materials and Methods.

a later section (see Discussion). Here we simply state that the peaks seen at 1623 and 1627 cm^{-1} are assigned to β-structures, and those at 1673 and 1687 cm^{-1} are assigned to antiparallel β-sheet, while the peak at 1650 cm^{-1} remains unassigned.

Circular Dichroism of Leu Peptide in Aqueous Solution. The spectra shown in Figure 4 give the concentration dependence of the circular dichroism spectra for the Leu peptide in 50 mM Tris buffer (see Materials and Methods). To allow measurements below 200 nm at the highest concentration of peptide, both the concentration of Tris buffer and the highest concentration of peptide were less than those used for the Ala peptide. There are two major differences apparent between the CD spectra for the Ala peptide (Figure 1) and for the Leu peptide (Figure 4). First, the general spectral shape of the traces in Figure 4 can be attributed to helical structures (Johnson, 1990), in contrast to the β-structure spectra obtained for the Ala peptide. It is possible that any β-structure signal for the Leu peptide is masked due to the smaller molar extinction coefficients for β-structures relative to helical structures (Urry, 1985).

The second difference concerns the spectral shape. The spectra for the Leu peptide change shape as a function of peptide concentration, showing shifts in maxima and relative amplitude changes. This is in contrast to the shapes of the Ala peptide spectra, which are the same at all concentrations. For the Leu peptide spectra (Figure 4), the maximum value shifts from approximately 190 nm at 0.5 mg/mL = 0.17 mM peptide and 0.1 mg/mL = 0.03 mM peptide (two bottom panels) to about 195−196 nm at 5 mg/mL = 1.7 mM peptide (top panel). CD spectra for helical structures usually have maxima between 194 and 198 nm, although experimental spectra with maxima below this range have been published (Zhou *et al.*, 1992). The blue-shift to 190 nm can be explained by the presence of unordered structures (Johnson,

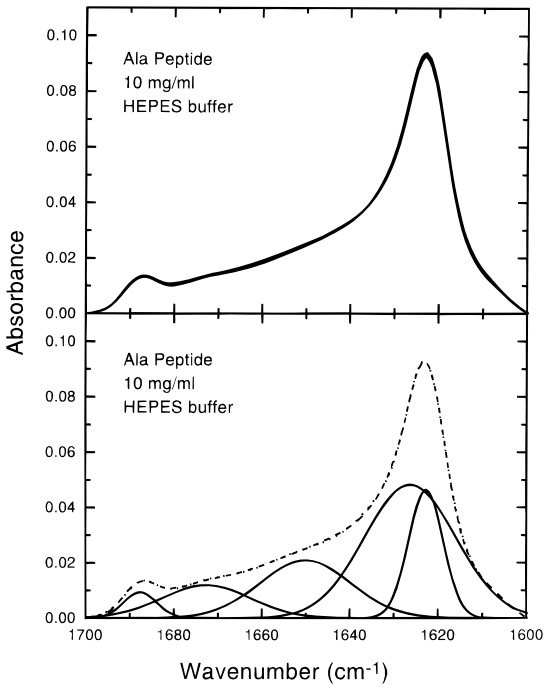

FIGURE 3: Temperature-dependent FTIR spectra and curve-fitted peaks for the Ala peptide (10 mg of peptide/mL = 3.5 mM Ala peptide) in D_2O buffer containing 100 mM HEPES, pD = 7.7. Top panel: Temperature dependence of FTIR spectra at 15, 25, 37, and 45 °C. Bottom panel: Curve-fitted peaks for Ala peptide FTIR spectra at 45 °C. The original spectrum is drawn using a dashed line (- - -), the sum of the curve-fitted peaks is drawn using a dotted line (•••), and the curve-fitted peaks are drawn using solid lines (—). Sample preparation, infrared measurements, and curve-fitting analysis procedures are described under Materials and Methods and Discussion. The final χ^2 value for the curve-fitting analysis of this spectrum was 2.1×10^{-5}.

1990), which would give a minimum in the appropriate range and account for the position at 190 nm. While the minimum at 222 nm shows no apparent shift, the lower wavelength minimum does seem to red-shift 1−2 nm as peptide concentration increases. A more obvious change is the ellipticity at 208 nm relative to 222 nm; the measured ellipticity at 208 nm shows a larger decrease as the peptide concentration increases compared to the minimum at 222 nm. At the lowest concentration of peptide (bottom panel) the minima are approximately equal with almost no rise in ellipticity between them. At 0.5 mg/mL Leu peptide (middle panel) the minima are approximately equal, while at the highest concentration of Leu peptide (top panel) the minimum at 208 nm is lower than the one at 222 nm. The shapes for the latter two spectra have been attributed to the presence of coiled-coil structures (Zhou *et al*., 1992; Graddis *et al*., 1993).

FTIR Spectroscopy and Curve-Fitting Analysis of Leu Peptide in Aqueous Solution. As for the Ala peptide, we collected ambient temperature FTIR spectra on the same Leu peptide samples prepared for circular dichroism. The results of the FTIR scans for the 5 mg/mL = 1.7 mM (top panel) and 0.5 mg/mL = 0.17 mM (bottom panel) concentrations of Leu peptide are presented in Figure 5. FTIR scans of the lowest concentration (0.1 mg/mL Leu peptide) did not give usable spectra. The concentration-dependent differences noted in the CD spectra (Figure 4) are apparent in the FTIR spectra for these samples; the FTIR spectral shape alters dramatically with concentration and the maximum absorbance shifts from approximately 1650 cm^{-1} at 5 mg/mL Leu peptide to below 1640 cm^{-1} at 0.5 mg/mL Leu peptide.

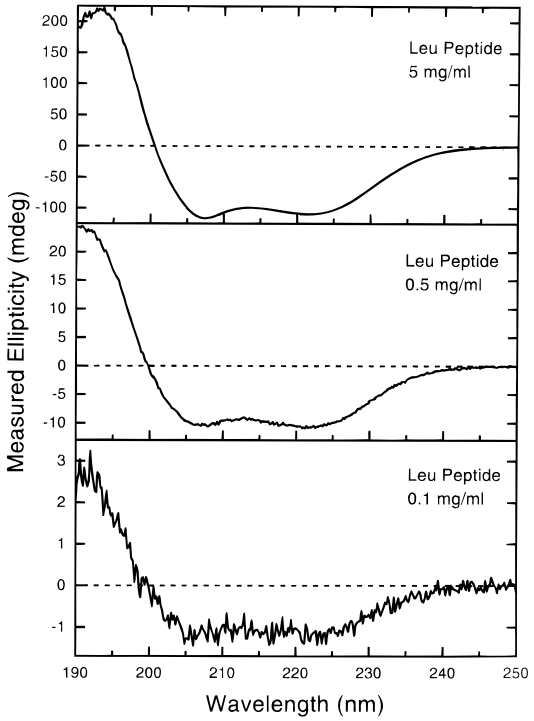

FIGURE 4: Concentration-dependent circular dichroism spectra for the Leu peptide at ambient temperature in D_2O buffer containing 50 mM Tris-HCl, pD = 7.7. Top panel: 5 mg of peptide/mL = 1.7 mM Leu peptide. Middle panel: 0.5 mg of peptide/mL = 0.17 mM Leu peptide. Bottom panel: 0.1 mg of peptide/mL = 0.03 mM Leu peptide. Sample preparation and CD measurements are described under Materials and Methods.

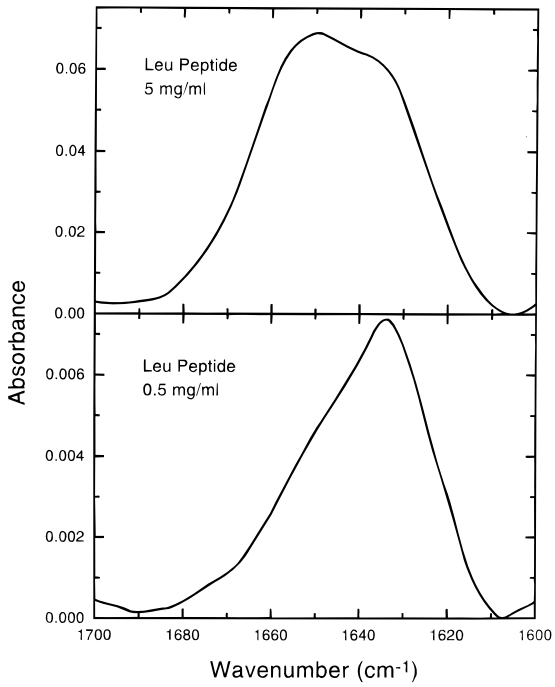

FIGURE 5: Concentration-dependent FTIR spectra for the Leu peptide at ambient temperature in D_2O buffer containing 50 mM Tris-HCl, pD = 7.7. Top panel: 5 mg of peptide/mL = 1.7 mM Leu peptide. Bottom panel: 0.5 mg of peptide/mL = 0.17 mM Leu peptide. Sample preparation and FTIR measurements are described under Materials and Methods.

Figure 6 shows the temperature dependence of the FTIR spectra for two different concentrations of the Leu peptide

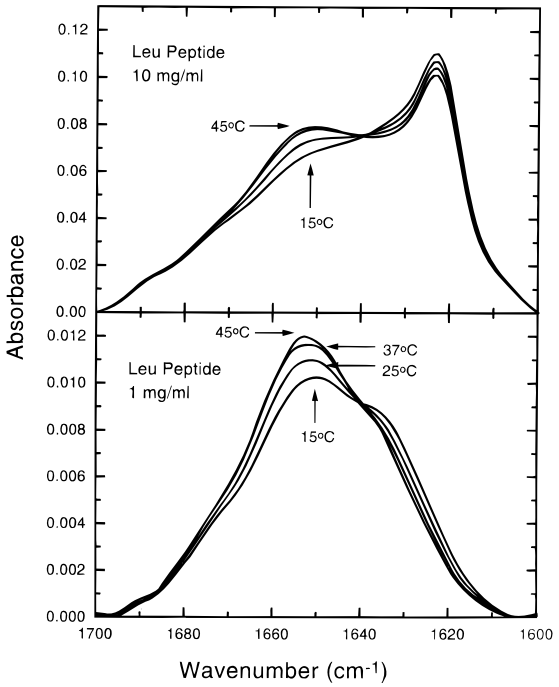

FIGURE 6: Temperature-dependent FTIR spectra for the Leu peptide in D_2O buffer containing 100 mM HEPES, pD = 7.7. Top panel: High-concentration spectra for Leu peptide (10 mg of peptide/mL = 3.4 mM Leu peptide). Bottom panel: Low-concentration spectra for Leu peptide (1 mg of peptide/mL = 0.34 mM Leu peptide). The arrows indicate spectra for different incubation temperatures. Sample preparation and infrared measurements are described under Materials and Methods.

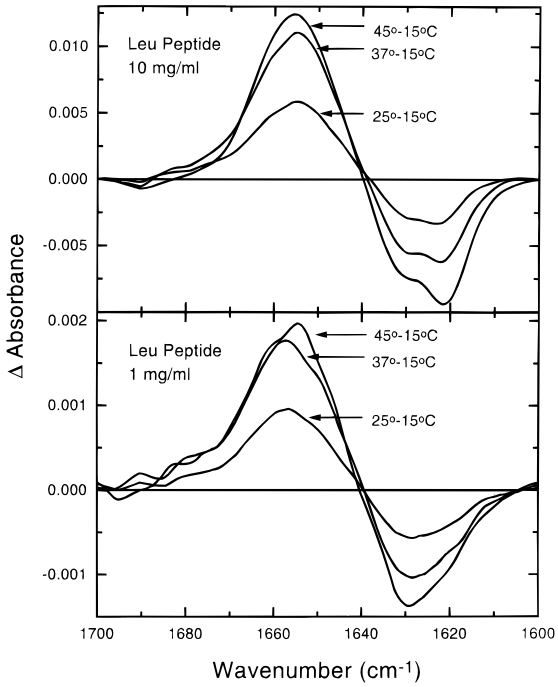

FIGURE 7: Difference FTIR spectra for the Leu peptide generated by subtraction of the 15 °C spectrum from spectra at higher temperatures. Top panel: 10 mg of peptide/mL = 3.4 mM Leu peptide. Bottom panel: 1 mg of peptide/mL = 0.34 mM Leu peptide. Annotated arrows indicate the temperatures corresponding to each difference spectrum.

in 100 mM HEPES buffer in D_2O at pD = 7.7. Samples were equilibrated at the given temperatures in a thermostated IR cell for 2−3 h before the scans were collected (see Materials and Methods). No hysteresis in spectral shape was seen; therefore, only one spectrum at each temperature is shown for clarity. Incubation times less than 2 h did result in hysteresis (results not shown), implying a slow kinetic equilibrium between the different solution structures of the peptide.

As seen in the FTIR spectra taken at ambient temperature (Figure 5), it is apparent that the spectra in Figure 6 for the two concentrations of Leu peptide, 1 mg/mL = 0.34 mM (bottom panel) and 10 mg/mL = 3.4 mM (top panel), differ; the higher concentration of Leu peptide has two distinct peaks, while the lower concentration has only a single peak with a shoulder. The spectra shown in Figure 6 also show a definite temperature dependence that was characteristic of the Leu peptide in aqueous buffer but disappeared when this peptide was bound to lipid vesicles (see below). To test whether the apparent isosbestic point at 1640 cm^{-1} did in fact exist, we subtracted the spectra collected at 15 °C from the higher temperature spectra for each concentration of Leu peptide (Williams *et al.*, 1996). The occurrence of a sharp isosbestic point would be indicated by the difference spectra for the various temperatures converging at $\Delta A = 0$. The results, plotted in Figure 7, do not support the existence of true isosbestic points, which would be strong evidence for a simple, two-state equilibrium between structures, at either concentration of Leu peptide.

Because the Leu peptide showed both temperature and concentration dependence, spectra for 10 and 1 mg/mL Leu peptide samples at 15 and 45 °C were analyzed to estimate the relative fluctuations in structures. Results for the curve-fitting analyses are shown in Figure 8 with individual parameters and the final structural assignments listed in Table 1. While the high-concentration spectra (10 mg/mL, left panels) require five curves for a reasonable fit ($\chi^2 < 6 \times 10^{-5}$), the low-concentration spectra (1 mg/mL, right panels) are fitted with only three curves. The need for additional peaks in the spectra obtained at 10 mg/mL peptide suggests the introduction of new structural types at the higher concentration of peptide. It is also possible that misleading artifacts were introduced during the water vapor subtraction or smoothing of the spectra (Jackson & Mantsch, 1995), although the consistent need for five curves at the high concentrations and only three at the lower concentrations of peptide to obtain good fits to the data make this unlikely. Details of the specific structural assignments for the peaks are given in a later section (see Discussion).

Temperature-Dependent FTIR Spectroscopy of Leu Peptide with Lipid Vesicles. The temperature dependence of the FTIR spectra (top panel) and curve-fitting analysis (bottom panel) for Leu peptide in the presence of 300 mM POPC LUV are shown in Figure 9 and the peak data are listed in Table 1. Binding curves show that, at 100 mM POPC LUV, the peptide is approximately 90% bound to lipid (Figure 10); therefore we assumed the peptide to be essentially all bound to the vesicles at 300 mM POPC. Since this lipid has a transition temperature (T_m) for the gel to the liquid crystal phase transition of −2 °C, the bilayer membranes were in the fluid phase throughout the temperature range studied.

The addition of lipid markedly affects the spectra for the Leu peptide, as is shown by comparing the top panels in Figure 6 (Leu peptide with no lipid) and Figure 9 (Leu peptide + 300 mM POPC vesicles). In the presence of lipid, the spectra have a single large peak at approximately 1653

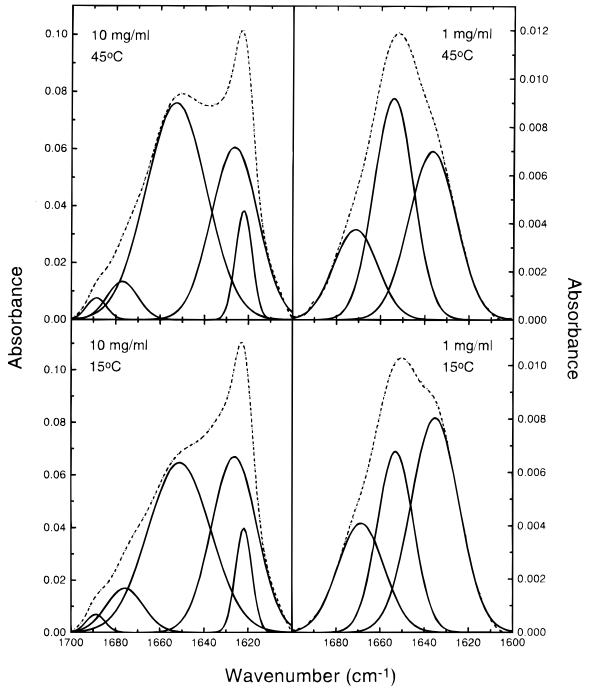

FIGURE 8: Curve-fitted peaks for the Leu peptide FTIR spectra in D_2O buffer at 45 °C (top panels) and 15 °C (bottom panels). The original spectra are drawn using dashed lines (- - -), the sums of the curve-fitted peaks are drawn using dotted lines (···), and the curve-fitted peaks are drawn using solid lines (—). Details of the curve-fitting analysis are described under Materials and Methods and Discussion. The final χ^2 values for the curve-fitting analysis of these spectra were 10 mg/mL Leu peptide $= 2.4 \times 10^{-5}$ and 2.3×10^{-5} for 45 °C and 15 °C, respectively, and 1 mg/mL Leu peptide $= 2.6 \times 10^{-7}$ and 2.2×10^{-7} for 45 °C and 15 °C, respectively.

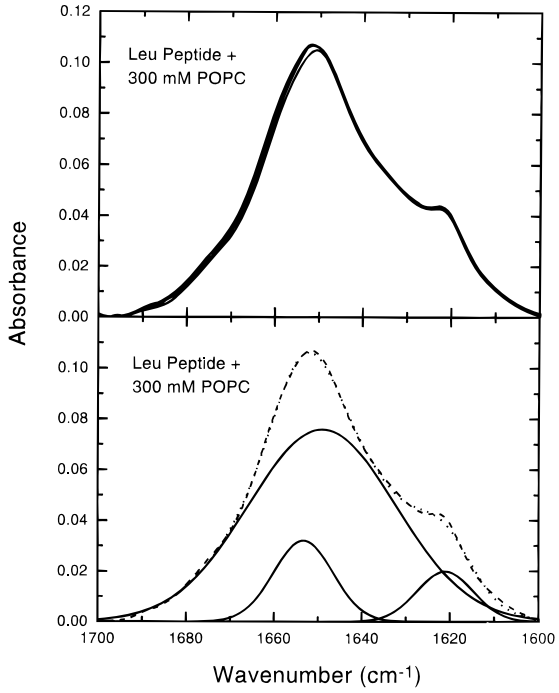

FIGURE 9: Temperature-dependent FTIR spectra and curve-fitted peaks for Leu peptide (10 mg of peptide/mL = 3.4 mM Leu peptide) in D_2O buffer containing 100 mM HEPES, pD = 7.7, with 300 mM POPC LUV. Top panel: Temperature dependence of FTIR spectra at 15, 25, 37, and 45 °C. Bottom panel: Curve-fitted peaks for Leu peptide with POPC vesicles FTIR spectra at 45 °C. The original spectrum is drawn using a dashed line (- - -), the sum of the curve-fitted peaks is drawn using a dotted line (···), and the curve-fitted peaks are drawn using solid lines (—). Sample preparation, infrared measurements, and curve-fitting analysis procedures are described under Materials and Methods and Discussion. The final χ^2 value for the curve-fitting analysis of the 45 °C spectra was 3.3×10^{-5}.

cm^{-1}, a small peak at 1622 cm^{-1}, and, most telling, no temperature-dependent changes in spectral shape. As for the Ala peptide, all the spectra overlay each other.

Due to the similarity of the spectra at all temperatures, only the curve-fit analysis of the spectra at 45 °C is shown (Figure 9, bottom panel). A new peak at 1649 cm^{-1} is now apparent. Although the separation between the two peaks at 1653 and 1649 cm^{-1} is small, curve-fitting analysis with only two peaks was unsatisfactory. As an additional control, we also measured the binding curves and FTIR spectra for the Ala peptide with POPC (results not shown). The Ala peptide remains unbound to the lipid at 100 mM POPC LUV (Figure 10) and the spectrum is essentially the same as for the Ala peptide in buffer alone.

Polarized ATR-IR of Leu Peptide with Supported Single-Lipid Bilayers. The orientation of lipid-bound Leu peptide was determined using polarized attenuated total internal reflectance infrared spectroscopy (ATR-IR) with single bilayers of POPC mounted on germanium plates. ATR-IR permits the orientation of molecules in a thin film to be estimated by exploiting the differential absorbance of aligned dipoles in polarized light [reviewed in Goormaghtigh and Ruysschaert (1990) and Fringeli (1993)]. Briefly, an order parameter and an angle with respect to the film normal are calculated from the ratio of the perpendicular and parallel absorbencies. While this calculated angle is an overall average of the total population present in the sample film and does not give information on the distribution of orientation angles, values close to 0° or 90° imply the majority of peptide has a single orientation. For peptides and proteins,

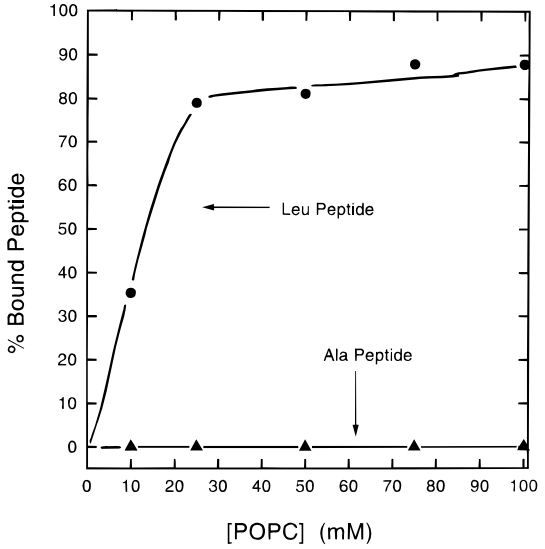

FIGURE 10: Binding curves for the interaction of the Leu peptide (circles) and the Ala peptide (triangles) with POPC LUV at 25 °C. Binding was performed in a D_2O buffer composed of 10 mM phosphate buffer and 100 mM NaF, pH = 7.5, using a centrifugation assay with approximate peptide concentrations of 1 mg/mL = 0.35 mM.

polarized ATR-IR is usually used in determining helix orientation, but the technique has also been applied to β-sheet structures (Rodionova *et al*., 1995).

Figure 11 shows the results of the polarized ATR-IR measurements at ambient temperature on single POPC

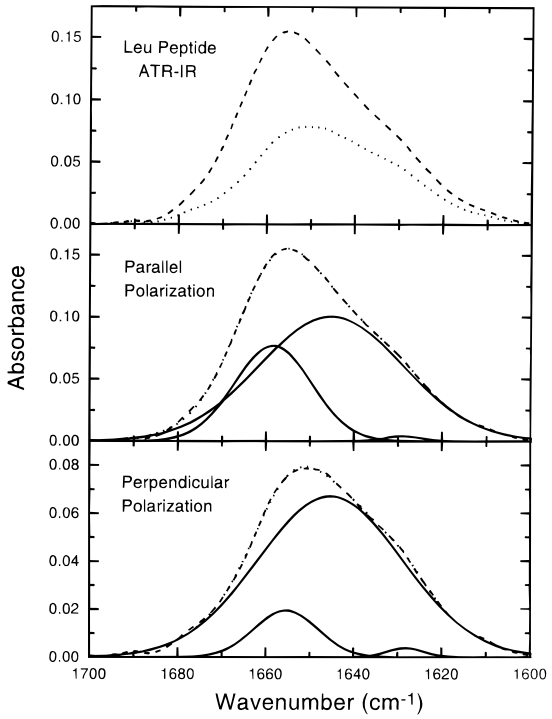

FIGURE 11: Polarized ATR-IR spectra and curve-fitted peaks for Leu peptide bound to a single supported planar bilayer of POPC. Top panel: Original spectra for parallel-polarized light (dashed line) and perpendicular-polarized light (dotted line) collected at ambient temperature. Middle panel: Curve-fitted peaks for parallel-polarized ATR-IR spectra. Bottom panel: Curve-fitted peaks for perpendicular-polarized ATR-IR spectra. The original spectra are drawn using dashed lines (- - -), the sums of the curve-fitted peaks are drawn using dotted lines (•••), and the curve-fitted peaks are drawn using solid lines (—). Sample preparation, infrared measurements, and curve-fitting analysis procedures are described in Materials and Methods and Discussion. The final χ^2 value for the curve-fitting analysis of these spectra were 5.6×10^{-5} and 3.5×10^{-5} for parallel and perpendicular polarizations, respectively.

bilayers using the Leu peptide. The original spectra are shown in the top panel while the curve-fitting results are shown in the middle panel (parallel polarization) and the bottom panel (perpendicular polarization) and listed in Table 1. Calculation of the helical angle with respect to the plane of the bilayer gave a perpendicular orientation for the long axis of the peptide helix. Details of the analysis used for helix orientation and an interpretation of the results are described in a later section (see Discussion).

DISCUSSION

This paper reports spectroscopic studies of two novel, *de novo* peptide sequences designed to insert spontaneously into lipid bilayer vesicles from aqueous solution. Below, the specific structure assignments for the peaks detected in the FTIR spectra and the ATR-IR calculations are discussed in detail. An interpretation of the temperature dependence is also included. Finally, the collective results of the solution and lipid-bound structural analyses are summarized in a tentative model for the binding and insertion of the Leu peptide into lipid bilayers. The rationale used in designing the peptide sequences is outlined in the Appendix.

Assignment of FTIR Peaks for the Ala Peptide in Solution. The correlation of IR peaks in the amide I region with different secondary and tertiary structures is complicated by the fact that structural assignments depend on the peptide or protein sequence, the type of solvent system (D_2O versus H_2O versus nonaqueous), the type of sample preparation (film, solution, mull, disk), and other environmental factors (dielectric constant of the medium, hydration of sample, etc.) (Jackson & Mantsch, 1995; Surewicz *et al*., 1993; Arrondo *et al*., 1993; Krimm & Bandekar, 1986; Fringeli & Gunthard, 1981). There is, however, one clear conclusion to be drawn from the Ala peptide data. Since the FTIR spectra in Figure 3 show no dependence on temperatures, the structures existing in solution do not change with temperature. Our structural interpretation of the IR peaks is as follows.

Five peaks resulted from the curve-fitting analysis of the Ala peptide in solution (Figure 3, bottom panel): 1623, 1627, 1650, 1673, and 1687 cm^{-1}. Peaks in the region of 1610−1640 cm^{-1} can be assigned to β-structures, including non-hydrogen-bonded structures such as turns, isolated strands, and strands on the edge of sheet structures, as well as hydrogen-bonded β-sheet, while the region for 1675−1695 cm^{-1} can be assigned to antiparallel β-sheet structure and aggregated strands (Jackson & Mantsch, 1995; Surewicz *et al*., 1993; Arrondo *et al*., 1993; Krimm & Bandekar, 1986; Fringeli & Gunthard, 1981). It is important to note that other types of structures, such as helical coiled-coils, also have strong absorbencies in this region (Heimburg *et al*., 1996; Reisdorf & Krimm, 1996) and structural assignments are aided by confirming methods such as CD spectroscopy. Therefore, with the exception of the 1650-cm^{-1} peak, we assigned the FTIR peaks to β-structures, basing this conclusion on both the peak positions and the CD spectra for the Ala peptide.

The assignment of the 1650-cm^{-1} peak is less obvious. Unordered structures in D_2O can give rise to two peaks, one at approximately 1650 cm^{-1} and one at about 1670 cm^{-1} (Chirgadze *et al*., 1973), and are generally assigned to peaks in the region of 1640−1650 cm^{-1} (Jackson & Mantsch, 1995; Surewicz *et al*., 1993; Arrondo *et al*., 1993; Krimm & Bandekar, 1986; Fringeli & Gunthard, 1981). The range cited for various helical structures, 1632−1670 cm^{-1} (Martinez & Millhauser, 1995; Jackson & Mantsch, 1995), overlaps this region and therefore either structural type can account for the peak seen at 1650 cm^{-1}. The CD spectrum for this peptide (Figure 1) shows no confirming evidence for either structure; ellipticity due to minor populations is conceivably masked by the absorbance from the large amount of β-structure present. Since no final conclusion can be drawn from the available data, this peak is left unassigned.

Assignment of FTIR Peaks for 1 mg/mL Leu Peptide in Solution. The temperature and concentration dependence of the Leu peptide spectra (Figures 4−7) reflect complex equilibria between multiple structures for this peptide. The assignment of peaks in the region of 1650−1660 cm^{-1} to helical structures is generally accepted, especially when confirmed by circular dichroism. The curve-fitted peak always seen in this range for the Leu peptide was therefore assigned to helix since all the CD spectra also show helical structure (Figure 4, see Results).

The assignments for the two other peaks seen at a lower concentration of Leu peptide (1 mg/mL; Figure 8, right panels) suggest the presence of at least three different structures at this concentration: extended unordered, helix (discussed above), and coiled-coil. Two curve-fit peaks at approximately 1670 and 1636 cm^{-1} are seen at both 15 °C (Figure 8, lower right panel) and 45 °C (Figure 8, upper

right panel) in the spectra for 1 mg/mL Leu peptide. A peak at 1669 cm^{-1} reported for poly(L-lysine) and poly(L-glutamic acid) in D_2O buffer was assigned to random-coil structure (Chirgadze *et al*., 1973). However, the pH at which these measurements were made, pH 6.0 and 7.0 for poly(lysine) and poly(glutamic acid), respectively, ensure that the peptides wee in a highly ionized state. Since these structures would be less compact than a true random unordered structure due to charge repulsion between ionized side chains, we classify this as an extended unordered structure. Supporting evidence for this unordered structure is given by the CD data (see Results). The maximum at 190 nm in the CD spectra at the lower concentrations of Leu peptide (Figure 4, bottom two panels) can be explained by the presence of unordered structure. In addition, the FTIR spectrum for the 0.5 mg/mL sample of Leu peptide (Figure 5, lower panel) has a strong maximum at approximately 1634 cm^{-1}. On the basis of the concentration-dependent shift of the 190-nm maximum, the relative amount of unordered structure should be greater at the lower concentrations of Leu peptide. The position of this FTIR peak in a region where β-structure peaks appear would reflect the extended nature of the unordered structure. We conclude that these two peaks can be ascribed to extended, unordered structure but that a coiled-coil structure also contributes.

Evidence for the presence of coiled-coil structure for the Leu peptide samples is given by both the CD spectra (Figure 4) and the curve-fitted peaks for the FTIR spectra (Figure 8). As discussed in Results, the CD spectra (Figure 4) fit a pattern of increasing coiled-coil structure with increasing concentration of Leu peptide. The direction of this concentration dependence would be expected for an equilibrium between monomeric helix and oligomeric coiled-coil structures. Recent evidence attributes three FTIR peaks at approximately 1650−1653, 1638−1640, and 1626−1630 cm^{-1} to coiled-coil structures (Heimburg *et al*., 1996; Reisdorf & Krimm, 1996). On the basis of these wavenumbers, we conclude that a coiled-coil structure contributes to, but is not solely responsible for, two of the three FTIR peaks detected at the 1 mg/mL concentration of Leu peptide.

Assignment of FTIR Peaks for 10 mg/mL Leu Peptide in Solution. A comparison of the FTIR spectra at different concentrations of Leu peptide shows that the large peak at 1622 cm^{-1} in the spectra for 10 mg/mL peptide (Figure 6, top panel) is not the same peak seen at 1634 cm^{-1} for 0.5 mg/mL peptide (Figure 5, bottom panel), suggesting the appearance of a new structure at the higher concentration of Leu peptide. The peak at 1622 cm^{-1} occurs at the same position as the major FTIR spectra peak for the Ala peptide, and the 10 mg/mL Leu peptide curve-fitting analysis gave peaks very similar to those for the Ala peptide. We conclude that β-structures similar to those of the Ala peptide occur at the high concentration of Leu peptide. The absence of clear β-structure in the CD spectra for the Leu peptide may be due to the large relative amounts of helical structure at all concentrations, which would mask the smaller ellipticity of the β-structures (Urry, 1985).

Evidence for the presence of coiled-coil structures at 5 mg/mL Leu peptide is seen in the CD spectrum (Figure 4, top panel; see Results); it is unlikely that the helical structures disappear when the peptide concentration is increased to 10 mg/mL. Therefore, we conclude that more than one structural type is contributing to a curve-fit peak. The final assignments are as follows: 1622 cm^{-1} = β-structure; 1627 cm^{-1} = β-structure + extended unordered + coiled-coil; 1651 (15 °C) and 1653 cm^{-1} (45 °C) = helix; 1676 (15 °C) and 1677 cm^{-1} (45 °C) = β-structure + extended unordered; 1689 (15 °C) and 1688 cm^{-1} (45 °C) = antiparallel β-sheet. The reasons for the extended unordered, helix, and coiled-coil assignments are the same as discussed for the 1 mg/mL Leu peptide spectra, while reasons for the specific assignments of β-structures are discussed in the Ala peptide section.

Assignment of FTIR Peaks for the Leu Peptide with 300 mM POPC Lipid Vesicles. We assigned the 1653-cm^{-1} peak to α-helix, presumably located in the hydrophobic domain of the peptide. The peak located at 1649 cm^{-1} is assigned to unordered structures, which are known to generate peaks in this region (Jackson & Mantsch, 1995). The small peak at 1622 cm^{-1} is attributed to the poly(lysine) portion of the peptide. This highly charged domain is expected to remain in or above the polar headgroup region of the lipid bilayer and, aside from proximity, have no direct interaction with the bilayer. Previous studies show no interaction of pentalysine peptides with zwitterionic phosphatydylcholine lipid vesicles (Kim *et al*., 1991). The corresponding peaks in the ATR-IR spectra were given the same assignments and are listed in Table 1.

Temperature Dependence of the Leu Peptide Structures. The curve-fitting analyses of the spectra for the Leu peptide (Figure 8) reveals that the peak assigned to helix structure always increases with an increase in temperature (Table 1). This increase is especially apparent in the 1 mg/mL Leu peptide spectra, where the helix peak area rises from 30% at 15 °C to 42% at 45 °C. The lack of a true isosbestic point (Figure 7) suggests that the temperature affects more than one equilibrium between structures. The results can be rationalized by an increase in monomeric helix due to two pathways: dissociation of coiled-coil structures and formation of helix from extended unordered structures due to hydrophobic interactions (Tanford, 1980). The spectra for the Ala peptide in solution do not exhibit a temperature dependence (Figure 3) and are mostly β-structure. The spectra for the Leu peptide, with a sequence substitution of three leucines for three alanine residues, shows a clear helical component. It is reasonable that the temperature dependence seen for the Leu peptide is due to the leucine residues acting as a nucleation center for helix formation. This tendency of leucine residues has been noted previously (Chou & Fasman, 1973) and the corresponding thermodynamic calculations have been reported recently (Creamer & Rose, 1995).

The hydrophobic nature of helix formation for the Leu peptide can also explain the data for the Leu peptide with 300 mM POPC vesicles. The temperature independence of these spectra with lipid vesicles (Figure 9, top panel) implies that the hydrophobic peptide interactions stabilizing the solution helical structures are not the same as the interactions stabilizing the lipid-bound structure; side-chain hydrophobic interactions are now replaced by peptide−lipid interactions.

Estimation of Leu Peptide Helix Orientation in LIpid Bilayers by Using ATR-IR. We used values of 29−34° for the transition moment of the poly(γ-benzyl-L-glutamate) helix in our calculations (Miyazawa & Blout, 1961), but we note that other values have been reported for symmetric polypeptides (Tsuboi, 1962; Bradbury *et al*., 1962). Using the 1656- and 1658-cm^{-1} peaks for perpendicular- and parallel-

polarized beams, respectively, helix order parameters of 1.0−0.85 from peak areas and 0.88−0.73 from peak heights were calculated. These values correspond to helical tilt angle ranges with respect to the plane of the bilayer of 90−72° for peak areas and 74−65° for peak heights. Values this close to 90° suggest that most of the helical peptide is oriented perpendicular to the plane of the lipid bilayer. An α-helix structure for the Leu_3-Ala_{22} sequence of the Leu peptide has a residue rise of 0.15 nm and thus a helical length of 3.75 nm, which is longer than the 2.58-nm thickness of the hydrophobic region of POPC bilayers (Nezil & Bloom, 1992). If a stiff, linear helix is assumed and this sequence spans the distance between the opposing hydrophilic/hydrophobic boundaries of the membrane, the peptide helix must be tilted at an angle of 43.5° with respect to the plane of the bilayer to fit within the hydrophobic core of the bilayer. The difference between the experimentally determined angles and this calculated value can be explained if several alanine residues reside outside the hydrophobic core of the bilayer, thus allowing the helix to extend slightly beyond the membrane surface and resulting in a nearly perpendicular orientation. This is the most likely orientation. It is also possible that the peptide can tilt, bend, and move within the bilayer (Vogel *et al*., 1988; Vogel, 1992), resulting in curved helices and a distribution of orientations. Peptide dimers may also form in the lipid bilayer, although larger aggregates are unlikely due to charge repulsion between poly(lysine) domains. A "ridges-into-grooves" packing of dimeric parallel helices can result in angles of 50° or 20° between helix long axes (Branden & Tooze, 1991). A final possibility may be that the peptide inserts as a helical hairpin with two antiparallel helical segments. However, such a helical hairpin structure would span little more than half of the bilayer, thus positioning the partial charges resulting from the helical dipole moments in the hydrophobic acyl chain region of the bilayer, an energetically unfavorable situation (Parsegian, 1969; Flewelling & Hubell, 1986).

A Tentative Molecular Model for the Interactions of Leu Peptide with Lipid Bilayers. A tentative model for Leu peptide binding to and inserting into POPC bilayers is shown in Figure 12. Our analysis of the data suggests that, in aqueous solutions, extended unordered peptide is in equilibrium with monomeric helical structures and oligomeric coiled-coils. The introduction of β-structure at the highest concentration of Leu peptide is excluded from the model since it is probably not a major component of the lipid binding. The lipid binding assays (Figure 10) used concentrations of Leu peptide, approximately 1 mg/mL = 0.34 mM, at which no appreciable β-structure is detected in the spectra. Increases in concentration of Leu peptide favor aggregation into coiled-coil structures while increases in both temperature and sequence hydrophobicity favor helix formation. These solution equilibria are shown in the upper part of Figure 12.

The interactions of the peptide with lipid bilayers are illustrated in the bottom portion of Figure 12. A peptide helix or helix aggregate, upon binding to the lipid bilayer, undergoes a change to an unordered structure. The basis for this transition may be the replacement of intrachain hydrogen bonding, which stabilizes the helical conformation, with hydrogen bonding between the peptide backbone and the phospholipid headgroups. The unordered structure then reverts to an α-helix as the peptide inserts with a transmembrane orientation into the bilayer. It is possible that an

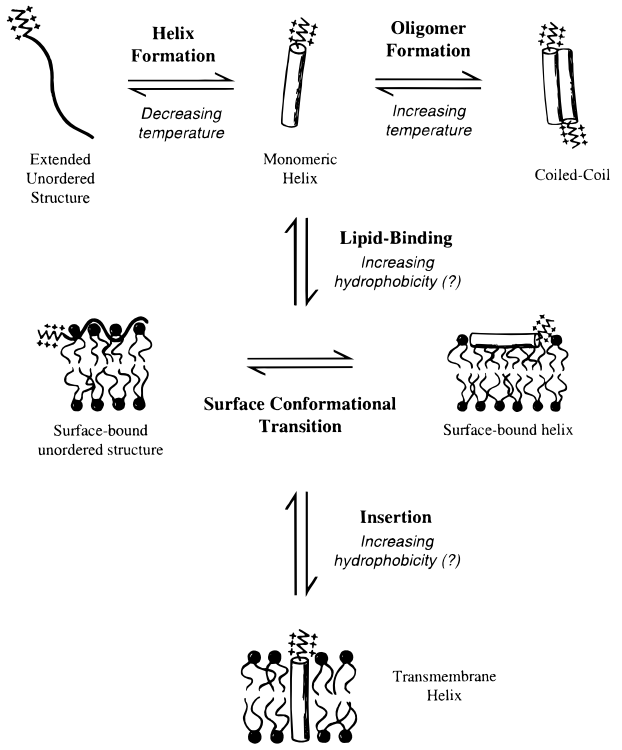

FIGURE 12: A proposed, simple model for the membrane binding and insertion of Leu peptide with POPC lipid bilayers suggested by the available data and analysis. It is possible that the various structures are connected by pathways other than those shown. Question marks indicate conditions that may have important effects on the equilibria and require further investigation. See text for discussion.

increase in sequence hydrophobicity increases the binding and/or the insertion of the peptide.

Support for this model, and its biological relevance, can be obtained from studies of biological proteins. As mentioned in the introduction, there is a class of protein sequences that partition nonspecifically into lipid bilayers both *in vitro* and, it is presumed, *in vivo* (Shore *et al*., 1995). Although the molecular mechanisms of the insertion process for even the best characterized of these proteins, cytochrome b_5, are poorly understood, a clear requirement is that the protein not form irreversible aggregates in solution. For both cytochrome b_5 and the designed peptides the stability of oligomeric structures is disrupted by charge repulsion between the hydrophilic domains (Calabro *et al*., 1976). A second clear requirement is the ability to bind to lipid; under the conditions of our experiments cytochrome b_5 would be completely bound to lipid at 1 mM POPC (Tretyachenko-Ladokhina *et al*., 1993), whereas we see complete binding for the Leu peptide only at concentrations greater than 50 mM POPC (Figure 6). The lipid binding correlates well with sequence hydrophobicity: the Ala peptide (no lipid binding) is less hydrophobic than the Leu peptide (lipid binding), which is less hydrophobic than the membrane-binding domain of cytochrome b_5 (strong lipid binding). Finally, the insertion of cytochrome b_5 does not require a protein conformational change and exhibits rapid kinetics; insertion is completed within seconds (Krishnamachary *et al*., 1994). In contrast, colicin A, a bacterial toxin that inserts spontaneously into lipid bilayers, requires a conformational change for membrane insertion and exhibits slow kinetics for this step (Gonzalez-Manas *et al*., 1992). Thus, the slow kinetics for the binding/insertion of the Leu peptide is consistent with

multiple structural changes for the peptide (surface-bound helix to surface-bound unordered to inserted helix) during the binding/insertion process.

On the basis of the above discussion, we propose that two significant factors for peptide and protein binding to membranes are inability to form irreversible aggregates and sequence hydrophobicity. Factors affecting insertion are sequence hydrophobicity and, in some cases, the ability to undergo conformational changes.

ACKNOWLEDGMENT

We gratefully acknowledge the assistance of Lukas K. Tamm, Suren A. Tatulian, and Cameron Grey for ATR-IR measurements; Peter W. Holloway, Robert W. Doebler, and Andrew R. G. Dibble for FTIR measurements; Linda Beggarly and the Biomolecular Research Facility at University of Virginia Health Sciences Center for automated peptide synthesis; and Ching-Hsien Huang for reviewing the manuscript.

APPENDIX

Rationale for Peptide Design. We established four major requirements for the peptide design. First, the peptide must be soluble in aqueous solution without the addition of detergents or organic solvents. Second, the peptide must partition readily into preformed lipid bilayers without the aid of a transmembrane potential, a change in pH, or the presence of cholesterol or other "helper" molecules. Third, the inserted peptide must not disrupt the lamellar structure of the lipid bilayer, as fusogenic peptides do. Fourth, the lipid-bound peptide must orient across the lipid bilayer in a transmembrane configuration rather than lying parallel to the bilayer plane. We also wanted the peptide to have well-defined secondary structure, simplifying biochemical and spectroscopic analyses, and be readily synthesized and purified in reasonable quantities. The first two requirements call for an amphiphilic structure with hydrophilic and hydrophobic sections. The third requirement omits two types of structures known to be fusogenic: amphiphilic helices with polar or charged residues grouped along one face of the helix and geometrically distorted helices with bulky residues clustered along one face (Eisenberg *et al*., 1984; White, 1990). The fourth requirement dictates a minimum peptide length; helices too short to span the bilayer in a stable secondary structure tend to orient parallel to the plane of the bilayer (Chung *et al*., 1992).

It was essential that the hydrophobic/hydrophilic features of the peptide be balanced so the peptide did not aggregate irreversibly in an insoluble complex or be too soluble to interact with the bilayer. Our structural paradigm was taken from fatty acids, lysolipids, and ionic detergents, all of which form soluble aggregates in aqueous solution and partition readily into lipid membranes. The linear peptide sequence was divided into two domains: a hydrophilic domain at the carboxyl terminus and a hydrophobic domain at the amino terminus. Another peptide designed to mimic a detergent has been reported previously (Schafmeister *et al*., 1993). However, this peptide was intended to solubilize membrane proteins rather than insert into lipid bilayers.

For the hydrophilic domain, a highly charged sequence was selected to both solubilize the peptide and destabilize any possible soluble peptide oligomers. Segregating hydrophilic and hydrophobic domains to opposite ends of the peptide made inhibition of peptide−lipid interactions by this sequence unlikely. A poly(lysine) sequence was chosen since these sequences are well-characterized regarding both their interactions with lipid bilayers (de Kruijff *et al*., 1985; Fukushijma *et al*., 1988; Anzai *et al*., 1991; Kim *et al*., 1991; Leckband *et al*., 1993) and their structures in solution as a function of pH (Venyaminow & Kalnin, 1990; Fasman *et al*., 1961; Townend *et al*., 1966; Greenfield *et al*., 1967; Greenfield & Fasman, 1969). Also, the surface binding of the peptide to bilayers can be increased by adding negatively charged lipid to the bilayer membrane preparations, a consideration for future experiments and applications.

We chose a helical secondary structure for the hydrophobic domain based on the following considerations. A theory of helix structure matching to bilayer thickness has been proposed [reviewed in Mouritsen and Bloom (1993)], allowing us to estimate a minimum peptide length. Furthermore, residues forming β-structures are difficult to incorporate in a growing peptide chain during the chemical synthesis due to interchain association, thus decreasing the synthetic yield (Bedford *et al*., 1990; Hyde *et al*., 1994). Because α-helical poly(alanine) and lipid molecules have similar diameters, this sequence was selected to minimize packing disruptions in the lipid bilayer. The structures of poly(alanine) under different conditions have been well-characterized (Elliott, 1954; Quadrifoglio & Urry, 1968; Masuda *et al*., 1969; Itoh & Shimanouchi, 1970; Urry *et al*., 1970; Frushour & Koenig, 1975; Dwivedi & Krimm, 1982, 1984) and two previous reports from this laboratory provided some information about poly(alanine)−lipid interactions (Chung & Thompson, 1994; Moll & Thompson, 1994). Some alanine residues were replaced with leucines to increase sequence hydrophobicity. The leucine residues were positioned to be on the trans side of the bilayer to that in which the peptide would presumably insert and far from the hydrophilic domain. To position the leucines in the acyl-chain region, two alanine residues were included to bridge the polar headgroup region.

The final sequence was selected to be H_2N-Ala_2-Leu_X-Ala_Y-Tyr-Lys_6-$CONH_2$, where *X* and *Y* can be varied to alter the hydrophobicity, and therefore the putative membrane partitioning, of the peptide sequence. A tyrosine was included between the hydrophobic and hydrophilic domains. Tyrosines, tryptophans, and phenylalanines are frequently found at the hydrophobic/hydrophilic interface of membrane proteins (Schiffer *et al*., 1992; Weiss *et al*., 1991). Although this is not an absolute requirement, we believed that a tyrosine would position the peptide in the lipid bilayer and, in addition, serve as an optical probe. Tryptophans were not considered for synthetic reasons. The amino terminus was left unmodified to serve as a reactive site for biochemical analysis.

REFERENCES

Anzai, K., Hamasuna, M., Kadono, H., Lee, S., Aoyagi, H., & Kirino, Y. (1991) *Biochim. Biophys. Acta 1064*, 256−266.

Arrondo, J. L. R., Muga, A., Castresana, J., & Goni, F. M. (1993) *Prog. Biophys. Mol. Biol. 59*, 23−56.

Bedford, J., Hyde, C., Johnson, T., Jun, W., Owen, D., Quibell, M., & Sheppard, R. C. (1990) *Int. J. Pept. Protein Res. 40*, 300−307.

Bradbury, E. M., Brown, L., Downie, A. R., Elliott, A., Fraser, R. D. B., & Hanby, W. E. (1962) *J. Mol. Biol. 5*, 230−247.
Branden, C., & Tooze, J. (1991) *Introduction to Protein Structure*, p 37, Garland Publishing, New York.
Calabro, M. A., Katz, J. T., & Holloway, P. W. (1976) *J. Biol. Chem. 251*, 2113−2118.
Chirgadze, Y. N., Shestopalov, B. V., & Yu, S. (1973) *Biopolymers 12*, 1337−1351.
Chou, P. Y., & Fasman, G. D. (1973) *J. Mol. Biol. 74*, 263−281.
Chung, L. A., & Thompson, T. E. (1994) *Biophys. J. 66*, A57.
Chung, L. A., & Thompson, T. E. (1995) *Biophys. J. 68*, A329.
Chung, L. A., & Thompson, T. E. (1996) *Biophys. J. 70*, A421.
Chung, L. A., Degrado, W. F., & Lear, J. D. (1992) *Biochemistry 31*, 6608−6616.
Creamer, T. P., & Rose, G. D. (1995) *Protein Sci. 4*, 1305−1314.
Crowley, K. S., Liao, S., Worrell, V. E., Reinhart, G. D., & Johnson, A. E. (1994) *Cell 78*, 461−471.
de Kruijff, B., Rietveld, A., Telders, N., & Vaandrager, B. (1985) *Biochim. Biophys. Acta 820*, 295−304.
Doebler, R., & Holloway, P. W. (1993) *Anal. Biochem. 212*, 562−564.
Dwivedi, A. M., & Krimm, S. (1982) *Macromolecules 15*, 186−193.
Dwivedi, A. M., & Krimm, S. (1984) *Biopolymers 23*, 923−943.
Eisenberg, D., Schwarz, E., Komaromy, M., & Wall, R. (1984) *J. Mol. Biol. 179*, 125−142.
Elliott, A. (1954) *Proc. R. Soc. London, Ser. A 226*, 408−421.
Fasman, G. D., Idelson, M., & Blout, E. R. (1961) *J. Am. Chem. Soc. 83*, 709−712.
Flewelling, R. F., & Hubbell, W. L. (1986) *Biophys. J. 49*, 541−552.
Frey, S., & Tamm, L. (1991) *Biophys. J. 60*, 922−930.
Fringeli, U. P. (1993) in *Internal Reflection Spectroscopy, Theory and Applications* (Mirabella, F. M., Jr., Ed.) pp 255−324, Marcel Dekker, New York.
Fringeli, U. P., & Gunthard, H. H,. (1981) in *Membrane Spectroscopy* (Grell, E., Ed.) pp 270−332.
Frushour, B. G., & Koenig, J. L. (1975) *Biopolymers 14*, 363−377.
Fukushima, K., Muraoka, Y., Inoue, T., & Shimozawa, R. (1988) *Biophys. Chem. 30*, 237−244.
Graddis, T. J., Myszka, D. G., & Chaiken, I. M. (1993) *Biochemistry 32*, 12664−12671.
Greenfield, N., & Fasman, G. D. (1969) *Biochemistry 8*, 4108−4116.
Greenfield, N., Davidson, B., & Fasman, G. D. (1967) *Biochemistry 6*, 1630−1637.
Gonzalez-Manas, J. M., Lakey, J. H., & Pattus, F. (1992) *Biochemistry 31*, 7294−7300.
Goormaghtigh, E., & Ruysschaert, J.-M. (1990) in *Molecular Description of Biological Membranes by Computer-Aided Conformational Analysis* (Brasseur, R., Ed.) Vol. I, pp 285−329, CRC Press, Boca Raton, FL.
Heimburg, T., Schuenemann, J., Weber, K., & Geisler, N. (1996) *Biochemistry 35*, 1375−1382.
Holloway, P. W., & Buchheit, C. (1990) *Biochemistry 29*, 9631−9637.
Hyde, C., Johnson, T., Owen, D., Quibell, M., & Sheppard, R. C. (1994) *Int. J. Pept. Protein Res. 43*, 431−440.
Itoh, K., & Shimanouchi, T. (1970) *Biopolymers 9*, 383−399.
Iwamoto, T., Grove, A., Montal, M. O., Montal, M., & Tomich, J. M. (1994) *Int. J. Pept. Protein Res. 43*, 597−607.
Jackson, M., & Mantsch, H. H. (1995) *Crit. Rev. Biochem. Mol. Biol. 30*, 95−120.
Johnson, W. C., Jr. (1990) *Proteins: Struct., Funct., Genet. 7*, 205−214.
Kim, J., Mosior, M., Chung, L. A., Wu, H., & McLaughlin, S. (1991) *Biophys. J. 60*, 135−148.
Krimm, S., & Bandekar, J. (1986) *Adv. Protein Chem. 38*, 181−364.
Krishnamachary, N., Stephenson, F. A., Steggles, A. W., & Holloway, P. W. (1994) *J. Fluoresc. 4*, 227−233.
Leckband, D., Chen, Y.-L., Israelachvilli, J., Wickman, H. H., Fletcher, M., & Zimmerman, R. (1993) *Biotechnol. Bioeng. 42*, 167−177.
Martinez, G., & Millhauser, G. (1995) *J. Struct. Biol. 114*, 23−27.
Masuda, Y., Fukushima, K., Fujii, T., & Miyazawa, T. (1969) *Biopolymers 8*, 91−99.
Miyazawa, T., & Blout, E. R. (1961) *J. Am. Chem. Soc. 83*, 712−719.
Moll, T. S., & Thompson, T. E. (1994) *Biochemistry 33*, 15469−15482.
Mouritsen, O. G., & Bloom, M. (1993) *Annu. Rev. Biophys. Biomol. Struct. 22*, 145−171.
Nezil, F. A., & Bloom, M. (1992) *Biophys. J. 61*, 1176−1183.
Ono, S., Lee, S., Mihara, H., Aoyagi, H., Kato, T., & Yamasaki, N. (1990) *Biochim. Biophys. Acta 1022*, 237−244.
Osterman, D. G., & Kaiser, E. T. (1985) *J. Cell. Biochem. 29*, 57−72.
Parsegian, V. A. (1969) *Nature 221*, 844−846.
Perczel, A., Park, K., & Fasman, G. D. (1992) *Proteins: Struct., Funct., Genet. 13*, 57−69.
Quadrifoglio, F., & Urry, D. W. (1968) *J. Am. Chem. Soc. 90*, 2755−2760.
Reisdorf, W. C., Jr. & Krimm, S. (1996) *Biochemistry 35*, 1383−1386.
Rodionova, N. A., Tatulian, S. A., Surrey, T., Jahnig, F., & Tamm, L. K. (1995) *Biochemistry 34*, 1921−1929.
Sander, C. (1991) *Curr. Opin. Struct. Biol. 1*, 630−637.
Schafmeister, C. E., Miercke, L. J., & Stroud, R. M. (1993) *Science 262*, 734−738.
Schiffer, M., Chang, C. H., & Stevens, F. J. (1992) *Protein Eng. 5*, 213−214.
Shore, G. C., McBride, H. M., Millar, D. G., Steenaart, N. A. E., & Nguyen, M. (1995) *Eur. J. Biochem. 227*, 9−18.
Surewicz, W. K., & Mantsch, H. H. (1989) *J. Mol. Struct. 214*, 143−147.
Surewicz, W. K., Mantsch, H. H., & Chapman, D. (1993) *Biochemistry 32*, 389−394.
Tanford, C. (1980) *The Hydrophobic Effect: Formation of Micelles and Bological Membranes*, 2nd ed., Wiley & Sons, New York.
Townend, R., Kumosinski, T. F., Timasheff, S. N., Fasman, G. D., & Davidson, B. (1966) *Biochem. Biophys. Res. Commun. 23*, 163−169.
Tretyachenko-Ladokhina, V. G., Ladokhin, A. S., Wang, L., Steggles, A. W., & Holloway, P. W. (1993) *Biochim. Biophys. Acta 1153*, 163−169.
Tsuboi, M. (1962) *J. Polymer Sci. 59*, 139−153.
Urry, D. W. (1985) in *Modern Physical Methods in Biochemistry, Part A* (Neuberger & Van Deenen, Eds.) pp 275−346, Elsevier, New York.
Urry, D. W., Hinners, T. A., & Krivacic, J. (1970) *Anal. Biochem. 37*, 85−91.
Vogel, H. (1992) *Q. Rev. Biophys. 25*, 433−457.
Vogel, H., NIlsson, L., Rigler, R., Voges, K. P., & Jung, G. (1988) *Proc. Natl. Acad. Sci. U.S.A. 85*, 5067−5071.
von Heijne, G. (1994) *FEBS Lett. 346*, 69−72.
Weiss, M. S., Abele, U., Weckesser, J., Welte, W., Schiltz, E., & Schulz, G. E. (1991) *Science 254*, 1627−1630.
White, J. M. (1990) *Annu. Rev. Physiol. 52*, 675−697.
Williams, S., Causgrove, T. P., Gilmanshin, R., Fang, K. S., Callender, R. H., Woodruff, W. H., & Dyer, R. B. (1996) *Biochemistry 35*, 691−697.
Zhou, N. E., Kay, C. M., & Hodges, R. S. (1992) *Biochemistry 31*, 5739−5746.

BI960080C